ACS APPLIED MATERIALS & INTERFACES

Research Article

www.acsami.org

Rationally Separating the Corona and Membrane Functions of Polymer Vesicles for Enhanced T_2 MRI and Drug Delivery

Jingya Qin,[†] Qiuming Liu,[†] Junxue Zhang,[†] Jing Chen,[†] Shuai Chen,[†] Yao Zhao,[§] and Jianzhong Du*[,†,‡]

[†]School of Materials Science and Engineering, Tongji University, 4800 Caoan Road, Shanghai 201804, China

[‡]Shanghai Tenth People's Hospital, Tongji University School of Medicine, 301 Middle Yanchang Road, Shanghai 200072, China

[§]Beijing National Laboratory for Molecular Sciences; CAS Key Laboratory of Analytical Chemistry for Living Biosystems; Beijing Center for Mass Spectrometry; Institute of Chemistry, Chinese Academy of Sciences, Beijing 100190, China

Supporting Information

ABSTRACT: It is an important challenge to in situ grow ultrafine super-paramagnetic iron oxide nanoparticles (SPIONs) in drug carriers such as polymer vesicles (also called polymersomes) while keeping their biodegradability for enhanced T_2-weighted magnetic resonance imaging (MRI) and drug delivery. Herein, we present a new strategy by rationally separating the corona and membrane functions of polymer vesicles to solve the above problem. We designed a poly(ethylene oxide)-*block*-poly(ε-caprolactone)-*block*-poly(acrylic acid) (PEO_{43}-*b*-PCL_{98}-*b*-PAA_{25}) triblock copolymer and self-assembled it into polymer vesicle. The PAA chains in the vesicle coronas are responsible for the in situ nanoprecipitation of ultrafine SPIONs, while the vesicle membrane composed of PCL is biodegradable. The SPIONs-decorated vesicle is water-dispersible, biocompatible, and slightly cytotoxic to normal human cells. Dynamic light scattering, transmission electron microscopy, energy disperse spectroscopy, and vibrating sample magnetometer revealed the formation of ultrafine super-paramagnetic Fe_3O_4 nanoparticles (1.9 ± 0.3 nm) in the coronas of polymer vesicles. Furthermore, the CCK-8 assay revealed low cytotoxicity of vesicles against normal L02 liver cells without and with Fe_3O_4 nanoparticles. The in vitro and in vivo MRI experiments confirmed the enhanced T_2-weighted MRI sensitivity and excellent metastasis in mice. The loading and release experiments of an anticancer drug, doxorubicin hydrochloride (DOX·HCl), indicated that the Fe_3O_4-decorated magnetic vesicles have potential applications as a nanocarrier for anticancer drug delivery. Moreover, the polymer vesicle is degradable in the presence of enzyme such as *Pseudomonas* lipases, and the ultrafine Fe_3O_4 nanoparticles in the vesicle coronas are confirmed to be degradable under weakly acidic conditions. Overall, this decoration-in-vesicle-coronas strategy provides us with a new insight for preparing water-dispersible ultrafine super-paramagnetic Fe_3O_4 nanoparticles with promising theranostic applications in biomedicine.

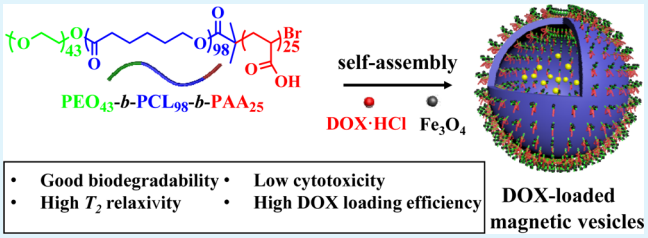

KEYWORDS: *vesicles, super-paramagnetic iron oxide nanoparticles, magnetic resonance imaging, self-assembly, drug delivery*

1. INTRODUCTION

Magnetic resonance imaging (MRI) is one of the most promising clinical imaging techniques in cancer diagnosis due to its high spatial resolution and noninvasive feature.[1,2] Benefiting from the various contrast agents, the sensitivity of MRI has been significantly enhanced since 20 years ago.[3] For example, positive contrast agents such as $[Gd(DTPA)]^{2-}$ complex (DTPA stands for diethylentriaminepentacetic acid) can shorten the longitudinal relaxation time T_1, expressed by the brightness.[4,5] In contrast, negative contrast agents such as super-paramagnetic iron oxide nanoparticles (SPIONs) are able to shorten the transverse relaxation time T_2, resulting in the darkening of the magnetic resonance images.[4,6−8]

However, recent studies revealed that some $[Gd(DTPA)]^{2-}$ complex may lead to toxicity and metabolic problems.[9−12] Furthermore, patients may suffer from nephrogenic systemic fibrosis (NSF, a rare and serious syndrome that involves fibrosis of skin, joints, eyes, and internal organs) if they frequently use gadolinium-based contrast agents.[12] On the contrary, SPIONs with large specific surface area and low cytotoxicity have attracted more and more attention as the contrast agents for MRI.[13,14] However, SPIONs have not been widely used in clinic in the past due to their poor water dispersibility and fast elimination through the reticuloendothelial system (RES), etc.[15] Therefore, water-dispersible polymeric nanocarriers have been employed to encapsulate Gd[16] or SPIONs for minimizing cytotoxicity and enhancing MRI.[1,17−19]

Over the past decades, polymeric drug delivery systems have shown promising potential applications in cancer therapy.[20] Lipids and polymers can provide passive targeting of anticancer drugs to tumor cells due to enhanced permeability and retention (EPR) effect.[21,22] For example, polymer vesicles

Received: April 14, 2015
Accepted: June 5, 2015
Published: June 5, 2015

DOI: 10.1021/acsami.5b03222
ACS Appl. Mater. Interfaces 2015, 7, 14043−14052

Scheme 1. Rationally Separating the Corona and Membrane Functions of a Multifunctional, Water-Dispersible, Biocompatible, Biodegradable, and Low-Cytotoxic Polymer Vesicle Self-Assembled from PEO_{43}-*b*-PCL_{98}-*b*-PAA_{25} Triblock Copolymer[a]

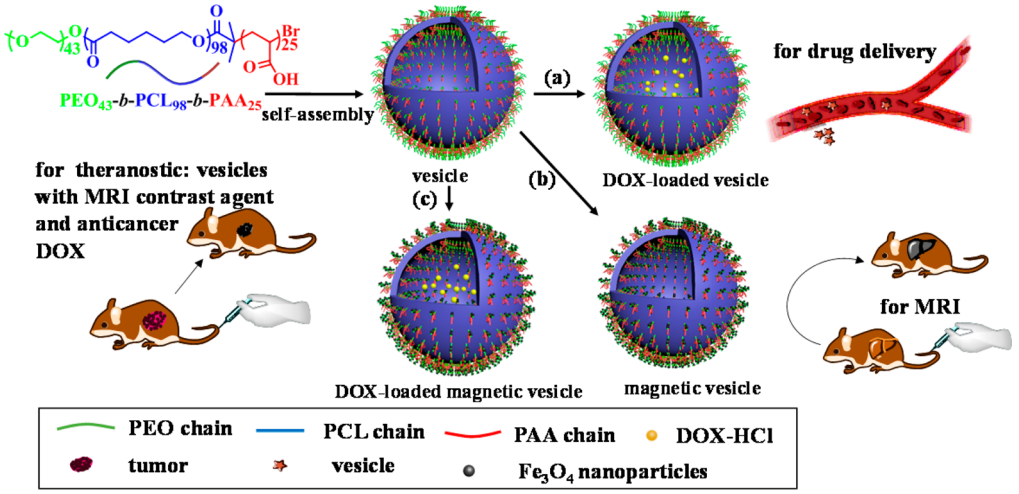

[a]The PAA chains in the vesicle coronas are responsible for the in situ deposition of ultrafine Fe_3O_4 nanoparticles, while the PCL vesicle membrane is biodegradable. (a) The triblock copolymer vesicles are a biocompatible and biodegradable drug delivery vehicle that can encapsulate and release anticancer drugs. (b) Magnetic vesicles decorated by ultrafine Fe_3O_4 nanoparticles can be used as an MRI contrast agent. (c) DOX-loaded magnetic vesicles can be used for cancer detection and therapy as a theranostic agent.

have been widely investigated because both hydrophilic and hydrophobic drugs can be loaded in the cavity and the membrane of vesicles, respectively.[20,23−25] Recently, smart polymer vesicles that can respond to physical or chemical stimuli exhibit great potential in controlled release of encapsulated drugs.[26−30] Moreover, they may be employed as an ideal delivery vehicle of SPIONs to solve the problems of stability and poor dispersibility.[31−35]Generally, SPIONs were preformed and then adsorbed in the vesicles.[36−38]

In 2012, our group reported an alternative method for effectively loading SPIONs by in situ precipitation of superparamagnetic Fe_3O_4 in the *membrane* of a pH-responsive vesicle self-assembled from poly(ethylene oxide)-*block*-poly(*tert*-butyl acrylate-*stat*-acrylic acid) [PEO-*b*-P(AA-*stat*-*t*BA)], leading to high loading efficiency, low cytotoxicity, excellent stability, and water solubility.[36] The key design principle is the rational engineering of the −COOH groups of PAA into the membrane of vesicle followed by subsequent deposition of Fe_3O_4 in the membrane. However, this method needs to sacrifice biodegradability of the membrane of vesicle. On the other hand, most of vesicle membranes constituted by biodegradable polymers are not able to in situ deposit superparamagnetic Fe_3O_4 nanoparticles. Till now, the simultaneous delivery of in situ precipitated SPIONs and anticancer drugs in a polymer vesicle with a biodegradable membrane still remains an important challenge.

Herein, we present a new strategy for balancing the in situ growth feasibility of SPIONs and the biodegradability of vesicles by rationally separating the corona and membrane functions of vesicles to solve the above problems and for enhanced MRI and anticancer drug delivery. The rationale of this strategy is shown in Scheme 1. Poly(ethylene oxide)-*block*-poly(caprolactone)-*block*-poly(acrylic acid) (PEO_{43}-*b*-PCL_{98}-*b*-PAA_{25}) triblock copolymer was synthesized and self-assembled into vesicles. The PCL chains are designed for forming the membrane of vesicle and for subsequent on-demand biodegradation in the presense of enzyme or acid. It is noteworthy that this PCL membrane is different from our previously reported P(AA-*stat*-*t*BA) membrane, which is only engineered for in situ deposition of SPIONs but not degradable.[36] The hydrophilic PEO and PAA chains are designed as the mixture vesicle coronas to stabilize vesicles in water. Moreover, the PAA vesicle coronas are designed for in situ growth of ultrafine SPIONs, which is different from our previous growth location (in the vesicle membrane).[36] Longer PEO coronas than PAA coronas are designed for increasing the biocompatibility of polymer vesicles but keeping the feasibility of deposition of SPIONs. More importantly, the SPIONs can be in situ grown in the PAA chains via chemical precipitation in the *preformed* DOX-loaded vesicles to form anticancer drug-loaded, water-dispersible, biodegradable, biocompatible, low-cytotoxic, superparamagnetic nanocarriers for enhanced MRI and anticancer drug delivery.

2. EXPERIMENTAL SECTION

2.1. Materials. Poly(ethylene oxide) methyl ether (MeO−PEO−OH; M_n = 1900) was purchased from Alfa Aesar and dried with toluene to remove traces of water by azeotropical distillation. The *tert*-butyl acrylate (*t*BA; purchased from Tokyo Chemical Industry Co., Ltd) monomer was purified through a silica column to remove inhibitor before use. *N*,*N*,*N*′,*N*″,*N*″-Pentamethyldiethylenetriamine (PMDETA; 98%) and 2-bromoisobutyryl bromide were obtained from Aladdin Chemistry, Co. (Shanghai, China). Trifluoroacetic acid (TFA), $FeCl_3{\cdot}6H_2O$, $FeCl_2{\cdot}4H_2O$, CuBr, tetrahydrofuran (THF), dichloromethane (DCM), and other reagents were purchased from Sinopharm Chemical Reagent Co., Ltd. (SCRC, Shanghai, China) and used as received.

2.2. Characterization. Dynamic light scattering (DLS) studies and the Zeta potential studies of aqueous polymer vesicle and magnetic vesicle solutions were determined using Nano-ZS 90 Nanosizer (Malvern Instruments Ltd., Worcestershire, U.K.) at a fixed scattering angle of 90°. The data were processed by cumulants analysis of the experimental correlation function. The vesicle diameters were calculated from the computed diffusion coefficients using the Stokes−Einstein equation. Each reported measurement was conducted for at least three runs.

Transmission electron microscopy (TEM) images, energy disperse spectroscopy (EDS), and electron diffraction were obtained using a

DOI: 10.1021/acsami.5b03222
ACS Appl. Mater. Interfaces 2015, 7, 14043−14052

JEM-2100 electron microscope operating at an acceleration voltage of 200 kV. TEM images of the vesicles prepared by PEO_{43}-*b*-PCL_{98}-*b*-PAA_{25} were observed according to our previous work.[39] Magnetic vesicles were not stained by any staining agent. EDS image was acquired from a part of the magnetic vesicle, while the electron diffraction image was obtained from the Fe_3O_4 nanoparticles.

Magnetic hysteresis loop of super-paramagnetic vesicles was determined by vibrating sample magnetometer (VSM). (Quantum Design). The hysteresis was obtained by varying H between +5000 and −5000 Oe at 300 K, and the comment time stamp is 3 630 430 780 s.

Iron Titration. The total iron concentration (mmol/L) was determined by an Agilent 7700 series inductively coupled plasma mass spectrometer (ICP-MS) after diluting the Fe_3O_4-decorated vesicle solution in HNO_3 (3%).

Fluorescence Experiments. Fluorescence experiments were measured to reveal the cumulative DOX release of DOX-loaded polymer vesicles (excitation at 461 nm and emission at 591 nm) via a Lumina fluorescence spectrometer (Thermo Fisher).

2.3. Synthesis of PEO_{43}-*b*-PCL_{98}-*b*-PAA_{25} Triblock Copolymer. PEO_{43}-*b*-PCL_{98}-*b*-PAA_{25} triblock copolymer was prepared and characterized according to a previously reported method.[39]

2.4. Self-Assembly of Copolymer into Vesicles. To prepare vesicles, PEO_{43}-*b*-PCL_{98}-*b*-PAA_{25} triblock copolymer (30 mg) was dissolved in 8.0 mL of THF and then added dropwise to the 16.0 mL of deionized water by a gas-tight syringe to form the vesicles. The vesicles were stirred for 30 min with continuous stirring of 150 r/min. Then the solution was transferred into a dialysis tube (cutoff M_n = 14 000) to dialyze against deionized water for 2 d by changing water three times per day to remove THF.

2.5. Preparation of Polymer Vesicles by in Situ Decoration of Super-Paramagnetic Fe_3O_4 Nanoparticles. The magnetic vesicles were prepared by chemical precipitation of Fe_3O_4 among the vesicle coronas according to our previous protocol.[36] First, the concentration of vesicles was diluted to 1.0 mg/mL. Second, to turn the carboxylic acid groups to carboxylate anions, the solution pH was tuned to neutral by adding the aqueous NaOH solution (pH 12). Third, the mixture solution (1.0 mL) with $FeCl_3{\cdot}6H_2O$ (0.55 mg) and $FeCl_2{\cdot}4H_2O$ (0.12 mg) was deoxygenated by bubbling argon for 30 min, which was then added into the vesicle solution (5.0 mL). Fourth, after the Fe^{3+} and Fe^{2+} ions were injected into the solution, the vesicle solution was stirred for 12 h under argon protection for ion exchange. Then the aqueous NaOH solution (pH 13, deoxygenated with argon) was added dropwise into the vesicle solution (with Fe^{3+} and Fe^{2+} ions) at room temperature. Finally, the reaction was performed at 60 °C for 2 h with stirring. The Fe_3O_4 nanoparticles were in situ deposited in the coronas of vesicles due to the electrostatic interactions between the carboxylic acid groups of PAA chains and the iron ions.

2.6. Preparation of Doxorubicin-Loaded Polymer Vesicles. PEO_{43}-*b*-PCL_{98}-*b*-PAA_{25} triblock copolymer (30.0 mg) was dissolved in THF (12.0 mL), and DOX·HCl (10.0 mg) was dissolved in deionized water (20.0 mL). The copolymer solution was added dropwise to the aqueous DOX·HCl solution within 0.5 h to form DOX-loaded polymer vesicles. After that, the unloaded free DOX and THF were removed by dialysis using a dialysis tube (cutoff M_n = 14 000) against 1000 mL of deionized water at 25 °C with 300 r/min of stirring. Deionized water was renewed five times in 2.5 h (every 0.5 h). The final volume of DOX-loaded polymer vesicle solution was 36.2 mL, and the amount of the drug encapsulated in the polymer vesicles was measured by fluorescence spectroscopy after dialysis.

The drug loading efficiency (DLE) and drug loading content (DLC) were calculated according to the following equations.

$$\mathrm{DLE}(\%) = \frac{\text{weight of drug encapsulated in vesicles}}{\text{weight of drug in feed}} \times 100$$

$$\mathrm{DLC}(\%) = \frac{\text{weight of drug encapsulated in vesicles}}{\text{weight of polymer}} \times 100$$

2.7. Preparation of Doxorubicin-Loaded Magnetic Vesicles. The above DOX-loaded vesicle solution (18.1 mL) was used for in situ chemical precipitation of Fe_3O_4 nanopaticles following the same method as mentioned in Section 2.5.

2.8. Loading of Anticancer Drug into the Preformed Magnetic Vesicles. The magnetic vesicle (15.0 mg in 15.0 mL of water) was mixed with DOX·HCl (5.0 mg in 3.0 mL of water) and stirred for 48 h to encapsulate the drug. Then the unloaded free drugs were removed by dialysis using a dialysis tube (cutoff M_n = 14 000) against 1000 mL of deionized water at 25 °C with 300 r/min of stirring. Deionized water was renewed five times in 2.5 h (every 0.5 h).

2.9. In Vitro Drug Release. The drug-release processes of the above three drug-loaded systems (Sections 2.6, 2.7, and 2.8) were performed by dialyzing 3.0 mL of DOX-loaded vesicles in the dialysis tube (cutoff M_n = 14 000) against 100 mL of tris(hydroxymethyl)-aminomethane (tris) buffer (0.01 M; pH 7.4) in a beaker (100 mL) at 37 °C and 200 r/min of stirring. At different time intervals, the release medium (3 mL) was withdrawn to determine the DOX concentration at 466 nm by fluorescence spectroscopy and then added into the beaker after measurement.

The cumulative DOX release was calculated according to the following formula:

$$\text{cumulative DOX release}(\%) = \frac{M_t}{M_0} \times 100$$

where M_t is the total amount of DOX released from vesicles at time t, and M_0 is the amount of DOX initially loaded into the vesicles.

A control DOX solution without any polymer vesicles was then prepared by adding 0.5 mg of DOX to 5.0 mL of water. The DOX solution was added to the dialysis tube and dialyzed against 100 mL of 0.01 M tris buffer at pH 7.4 and 37 °C. After different time intervals, 3.0 mL of tris buffer was periodically removed to determine the DOX concentration at 466 nm by fluorescence spectroscopy. Finally, the cumulative release curve of the free DOX was obtained.

2.10. Cytotoxicity Test. The cytotoxicity test of the magnetic polymer vesicles against L02 human normal liver cells was determined by measuring the inhibition of the cell growth using a Cell Counting Kit-8 (CCK-8) assay. L02 cells were first seeded in a 96-well plate at a density of 5000 cells/well and incubated overnight at 37 °C. Then, the cells were incubated with various concentrations of magnetic vesicles (5.0, 10.0, 20.0, 40.0, 100, 200, 500, and 1000 μg/mL) for 24, 48, and 72 h, respectively. Thereafter, each well was replaced by 100 μL of fresh media. The background absorbance at 450 nm (time 0 after CCK-8 was added) was removed from the absorbance after 1 h of incubation with CCK-8. The cell viability was obtained by calculating the amount of the formazan dye generated by the activity of dehydrogenases in cells because it is directly proportional to the number of living cells.

2.11. T_2 Relaxivity Measurement. The transverse relaxation time of Fe_3O_4-decorated vesicle solution was measured at 37 °C using a 1.41 T minispec mq 60 NMR Analyzer (Bruker, Germany). Relaxivity value was revealed via linear least-squares fitting of $1/T$ relaxation time (s^{-1}) versus the Fe concentration (millimolar).[40]

2.12. In Vitro and in Vivo Magnetic Resonance Imaging. The T_2 weights of the magnetic vesicle solution at various concentrations were measured with a GE Discovery MR 750 3.0 T clinical instrument at room temperature. The transverse T_2 measurements were obtained by using a multiple spin−echo two-dimensional (2D) imaging sequence (TR = 3500 ms, TE = 102 ms, SL = 2.0 mm).

Furthermore, normal little mice (C57BL/6 male, ∼25.5 g) were employed for in vivo MRI test of the magnetic vesicles. The mice were first injected the pentobarbital sodium (0.15 mL), and then the controlled image was acquired at room temperature using GE Discovery MR 750 3.0 T clinical instrument (FOV = 14 × 14 cm, SL = 1.0 mm, TR = 8444 ms). The Fe_3O_4-decorated magnetic vesicles were injected via the tail vein into the mice. Images were obtained at different time intervals after the injection of magnetic vesicles.

2.13. In Vitro Degradation of Vesicles. The aqueous lipase solution was added into the Fe_3O_4-decorated polymer vesicle solution

DOI: 10.1021/acsami.5b03222
ACS Appl. Mater. Interfaces 2015, 7, 14043−14052

and the pure polymer vesicle solution at the same given concentrations of lipase (0.025, 0.05 mg/mL) and polymer vesicle (0.05, 0.10 mg/mL), and then both mixtures were placed into an incubator at 37 °C to study the changes of the count rate with time. Finally, the solution was degraded into PEO, PAA, and hydroxyl carboxylic acid after several days.

2.14. Acid Degradation of Fe_3O_4 Nanoparticles in the Magnetic Vesicles. The acid degradation of Fe_3O_4 was performed by dialyzing Fe_3O_4-decorated magnetic vesicles (3.0 mL) in the dialysis tube (cutoff M_n = 14 000) against tris buffer (100 mL; 0.1 M; pH 5.0) in a beaker (100 mL) at 37 °C. At different time intervals, the buffer solution (2 mL) outside the dialysis tube was taken out to measure the concentration of Fe using ICP-MS, and another 2 mL of fresh buffer was added into the beaker after that. The concentration of Fe corresponds to the degraded Fe_3O_4 in the magnetic vesicles. According to the following formula, the weight of the degraded Fe_3O_4 is proportional to the weight of Fe ions in buffer, which means that the degradation rate of Fe_3O_4 is equal to the increase rate of the Fe ions in the buffer.

$$M_n = C_n \times V_n + V_t \times \sum_{i=1}^{n-1} C_{n-i}$$

$$\text{weight of the degraded } Fe_3O_4 = \left(\frac{\text{weight of Fe ions in buffer}}{M_{Fe}}\right) \times \frac{1}{3} \times M_{Fe_3O_4}$$

where M_n is the weight of the Fe ions at each time, and C_n is the concentration of Fe measured by ICP-MS. V_n is the volume of the buffer solution in the beaker. V_t is the volume of the buffer solution (2.0 mL) taken out, while n means the number of times that taken out from the beaker. M_{Fe} and M_{Fe3O4} are the relative molecular mass of Fe and Fe_3O_4, respectively.

3. RESULTS AND DISCUSSION

3.1. Self-Assembly of PEO_{43}-*b*-PCL_{98}-*b*-PAA_{25} Triblock Copolymer. PEO_{43}-*b*-PCL_{98}-*b*-PAA_{25} triblock copolymer was prepared according to a previously reported method.[39] The copolymer was self-assembled into vesicles with the PCL chains forming the biodegradable membrane and the PEO, PAA chains forming the coronas of the vesicle. As shown in curve (a) of Figure 1, the *z*-averaged hydrodynamic diameter (D_h) of the pure vesicles in aqueous solution is 138 nm, and the polydispersity (PDI) is 0.037 at pH 5.9 as determined by DLS. Furthermore, TEM study confirmed the hollow structure of vesicles (Figure 2A).

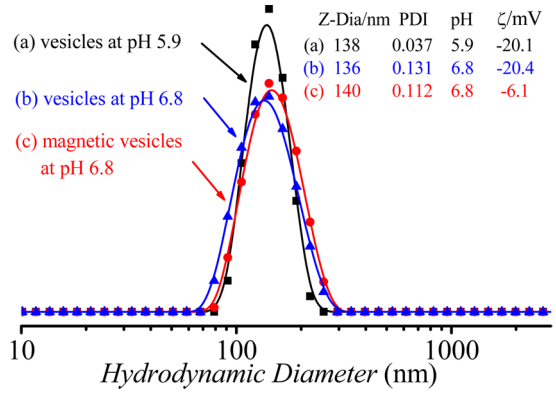

Figure 1. Intensity-averaged size distribution and zeta potential (by DLS) of PEO_{43}-*b*-PCL_{98}-*b*-PAA_{25} triblock copolymer vesicles before and after in situ decoration of super-paramagnetic Fe_3O_4 nanoparticles. (a) Pure vesicles without SPIONs at pH 5.9; (b) Pure vesicles without SPIONs at pH 6.8 and (c) Vesicles decorated with SPIONs in the coronas at pH 6.8. The vesicle concentration is 1.0 mg/mL.

3.2. Preparation of Super-paramagnetic Fe_3O_4 Decorated Vesicles via Chemical Precipitation. The Fe_3O_4-decorated super-paramagnetic vesicles were prepared by in situ chemical precipitation of iron oxides in the coronas of polymer vesicles. After tuning the vesicle solution pH to 7, the proper molar ratio of Fe^{2+}/Fe^{3+} concentrations was designed to interact with carboxylate anions of PAA in the vesicle coronas. When the molar ratio of $Fe^{3+}/-COO^-$ was 1/4.7 and the molar ratio of Fe^{3+} to Fe^{2+} was 1/3, the Fe_3O_4-decorated super-paramagnetic vesicles possessed nearly the strongest magnetism.[36,41,42] Then the Fe_3O_4 nanoparticles were in situ precipitated among the coronas of the vesicles by adding aqueous NaOH solution. With the alkaline solution being dropped, the mixture immediately turned light green, then gradually turned yellow, and eventually became the light brown solution within 2 h when stirred at 60 °C, indicating the formation of the Fe_3O_4-decorated super-paramagnetic vesicles.

Figure 3 shows the different macroscopic views between the magnetic vesicle solution with and without the external magnetic field. The Fe_3O_4 nanoparticles aggregated together with an external magnetic field. The magnetic vesicles can be well-redispersed after slight shaking.

ICP-MS measurement was used to further calculate the content of iron oxide nanoparticles in the super-paramagnetic polymer vesicles. The total iron concentration of magnetic vesicles is 0.648 mmol/L, and 3.0% Fe_3O_4 was decorated on the vesicle coronas. It was slightly lower than the theoretical value of 5.0%, probably due to the oxidation of the Fe^{2+}. Nevertheless, the 3.0% Fe_3O_4 content was enough for MRI.[43]

3.3. Dynamic Light Scattering and Transmission Electron Microscopy Studies of Super-Paramagnetic Vesicles. DLS and TEM studies were conducted to reveal the size and the morphology of the Fe_3O_4-decorated super-paramagnetic vesicles. Figure 1 shows the DLS studies on the polymer vesicles prepared from PEO_{43}-*b*-PCL_{98}-*b*-PAA_{25} copolymer before and after Fe_3O_4 decoration. The D_h of the magnetic vesicles became 140 nm with the PDI increased from 0.037 to 0.112, while the zeta potentials (ζ) of both kinds of vesicles were also changed from −20.4 mV at pH 6.8 to −6.1 mV at pH 6.8 due to the interactions between Fe^{3+}/Fe^{2+} and carboxylate anions on the vesicle coronas.

As shown in Figure 2B−D, ultrafine Fe_3O_4 nanoparticles were successfully deposited in the coronas of the polymer vesicles. The size of the Fe_3O_4 nanoparticles was estimated 1.9 ± 0.3 nm (Figure 2E), which is consistent with their super-paramagnetic behavior (usually less than 10 nm).[44] Figure 2G,H imitates the collapse of the Fe_3O_4-decorated vesicles, while the former one presents laterodeviation when vacuumized during the electron microscope operating.

The EDS shows the composition of Fe in the vesicles (Figure 4). The electron diffraction (ED) pattern in Figure 2F indicated the crystal structure of Fe_3O_4 nanoparticles. The interplanar crystal spacings were determined by measuring the distance of the diffraction rings. As shown in Table 1, the actual interplanar crystal spacing values match the theoretical ones of Fe_3O_4 crystals, further confirming the successful deposition of Fe_3O_4 nanocrystals in the vesicle coronas.

Moreover, the super-paramagnetic vesicle solution under an external magnet field (Figure 3c) was much more clear than the polymer vesicles of light blue (Figure 3a), proving that the

DOI: 10.1021/acsami.5b03222
ACS Appl. Mater. Interfaces 2015, 7, 14043−14052

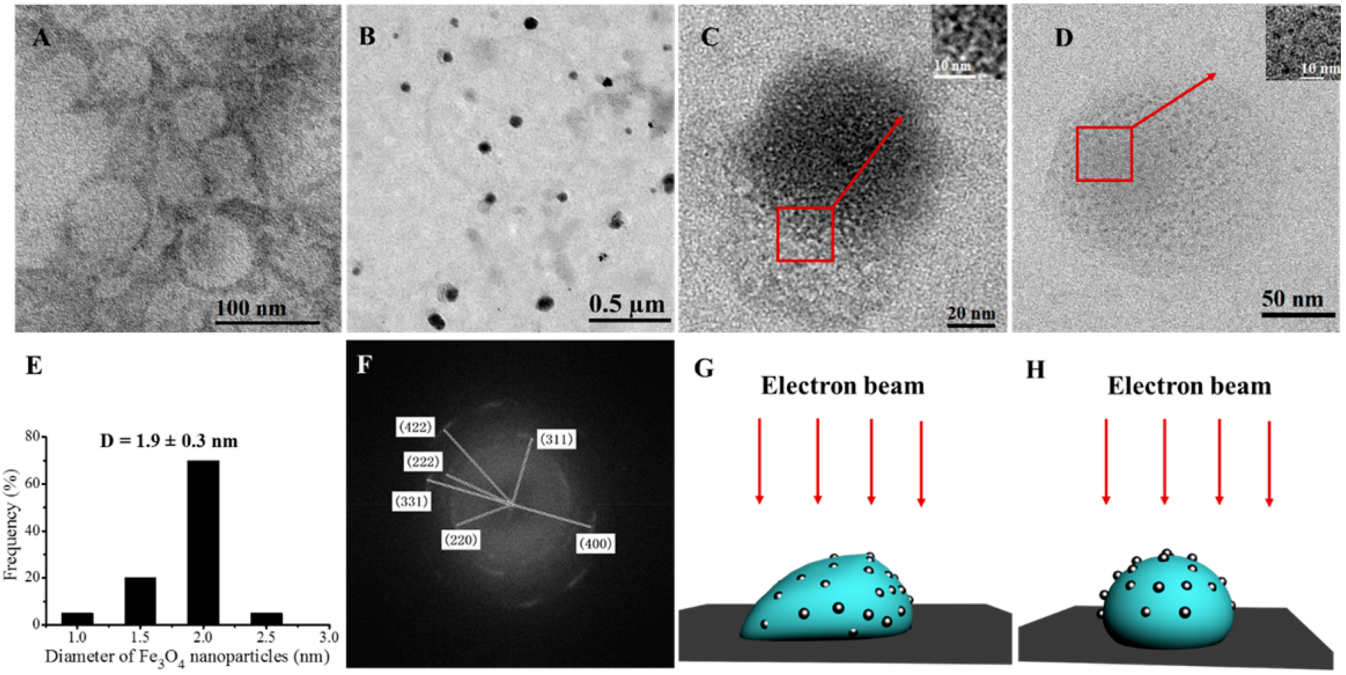

Figure 2. TEM images (A–D), TEM imaging simulation (G, H), and electron diffraction pattern (F) of vesicles prepared by PEO_{43}-*b*-PCL_{98}-*b*-PAA_{25} copolymer. (A) TEM images of vesicles before decoration with Fe_3O_4 nanoparticles. (B–D) TEM images of vesicles with Fe_3O_4 nanoparticles decorated in the coronas of vesicles. Magnified images in (C, D) confirmed the ultrafine nanostructure of Fe_3O_4 nanoparticles in the vesicles. (E) The size distribution of Fe_3O_4 nanoparticles. (F) The electron diffraction pattern of vesicles reveals the crystal structure of Fe_3O_4 nanoparticles. (G, H) Simulation of Fe_3O_4-decorated magnetic vesicles in (C, D) at different collapsed states, respectively.

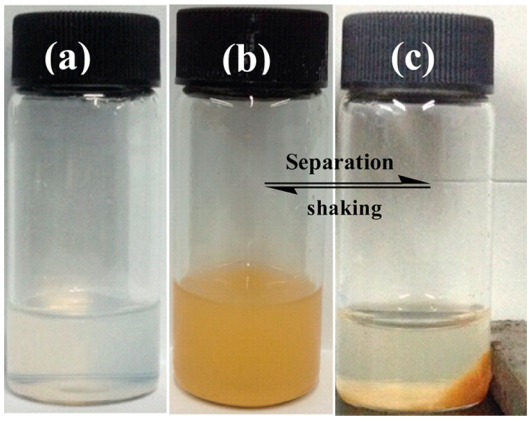

Figure 3. A macroscopic view of polymer vesicles (a) before and (b) after Fe_3O_4 decoration. (b) Superparamagnetic polymer vesicles without and (c) with an external magnetic field.

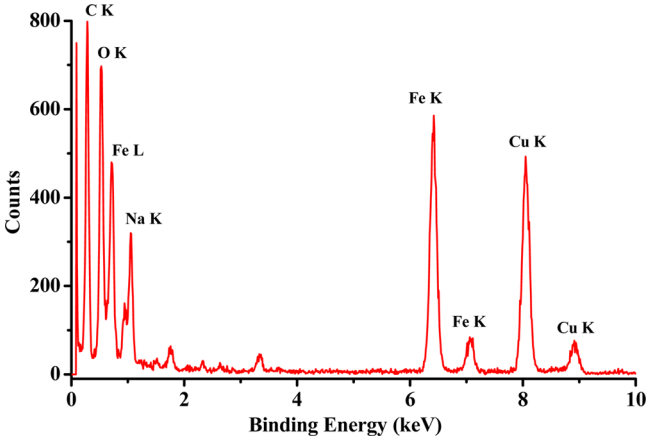

Figure 4. Energy disperse spectroscopy of magnetic vesicles.

Fe_3O_4 nanoparticles was deposited on the vesicles and not in the solution.

3.4. Magnetic Hysteresis Hoop of Magnetic Vesicles. The magnetic hysteresis hoop was measured by VSM. The S-like curve of Figure 5 confirmed that the magnetic vesicles have no remanence and coercivity at 300 K, indicating that the Fe_3O_4-decorated vesicles exhibit a super-paramagnetic behavior.[45] The specific saturation magnetization of magnetic vesicles is 0.314 emu per gram of the total mass of magnetic vesicles, which is equal to 10.5 emu per gram of pure Fe_3O_4 nanoparticles considering 3.0% of loading content. This value (10.5 emu/g) is bigger than 4.62 emu/g for the Fe_3O_4 nanoparticles[46] but smaller than bulk Fe_3O_4 (92 emu/g), possibly due to the much smaller size of the Fe_3O_4 nanocrystals and the existence of the organic polymer chains of vesicles.

Table 1. Comparison between the Actual and the Theoretical Values Obtained from Electron Diffraction of Fe_3O_4 Nanoparticles[a]

$d(A)_{real}$	$d(A)_{theor}$	*h*	*k*	*l*
2.931	2.966	2	2	0
2.477	2.529	3	1	1
2.422	2.422	2	2	2
2.061	2.097	4	0	0
1.958	1.924	3	3	1
1.707	1.712	4	2	2

[a] $d(A)_{real}$ and $d(A)_{theor}$ are the actual and theoretical values of the interplanar crystal spacing, respectively. *h*, *k*, *l*: indices of crystal face.

3.5. Cytotoxicity Study. The cytotoxicity of the Fe_3O_4-decorated super-paramagnetic vesicles against normal human

DOI: 10.1021/acsami.5b03222
ACS Appl. Mater. Interfaces 2015, 7, 14043–14052

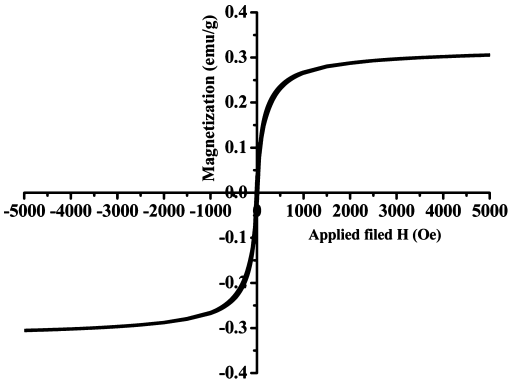

Figure 5. Magnetic hysteresis hoop of Fe_3O_4-decorated super-paramagnetic polymer vesicles at 300 K. The specific saturation magnetization value is relative to the mass of magnetic vesicles.

L02 liver cells was determined using a CCK-8 assay. L02 cells were incubated with various concentrations of the magnetic vesicle solutions for 24, 48, and 72 h. As shown in Figure 6,

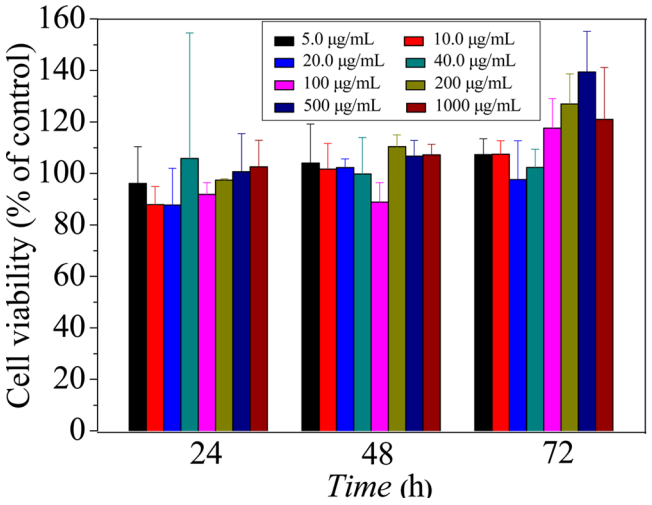

Figure 6. Cell viability of normal human L02 liver cells incubation with Fe_3O_4-decorated magnetic vesicles at different concentrations after 24, 48, and 72 h.

with the increase of the concentration of the Fe_3O_4-decorated vesicles, the cell viability was almost above 90% at 24 h. Even after 72 h, a significant decrease in cell viability was not observed at all of the concentrations of the magnetic vesicles, indicating that the magnetic vesicles did not obviously affect the viability of L02 cells. Therefore, the Fe_3O_4-decorated magnetic vesicles are slightly cytotoxic and may have potential biomedical applications.

Also, the cell viability of Hela cells in the presence of DOX-loaded vesicles without SPIONs was reported in our previous study,[16] showing excellent antitumor activity of DOX-loaded vesicles. In this paper, only 3.0% of SPIONs were in the vesicles, which may also keep similar antitumor property of DOX-loaded magnetic vesicles.

3.6. In Vitro and in Vivo Magnetic Resonance Imaging. In general, longitudinal relaxivity (r_1) and transverse relaxivity (r_2) are applied to evaluate the ability to alter spin−lattice relaxation (T_1) and spin−spin relaxation (T_2) in the MRI, respectively.[47] According to the previous reports, SPIONs can shorten the T_2 relaxivity value and enhance the negative contrast signal of MRI, which makes the images darker than that without an MRI contrast agent.[40,47−49] Figure 7 reveals the magnetic vesicles with an r_2 value of 108.4 mM^{-1} s^{-1}, which is slightly higher than that of a clinically used Feridex (105 mM^{-1} s^{-1}).[50]

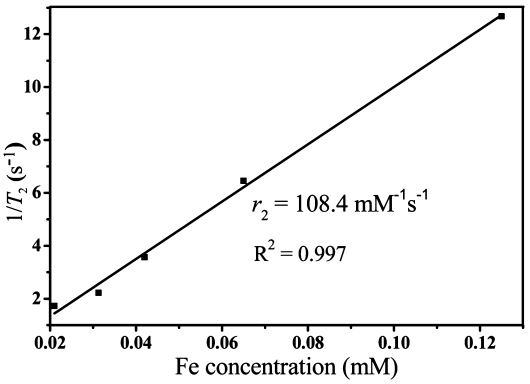

Figure 7. T_2 relaxation rate ($1/T_2$) as a function of iron concentration recorded for the aqueous vesicle solutions decorated with ~3.0 wt % super-paramagnetic Fe_3O_4 nanopaticles.

It is noteworthy that the amount of SPIONs in the vesicles is lower than that reported in our previous paper.[36] Furthermore, the size of vesicles in this paper is smaller than that in our previous paper, leading to the lower T_2 relaxivity value.[36] However, the vesicles in this paper may provide advantages such as excellent water dispersibility, biocompatibility and biodegradability, and low cytotoxicity.

Furthermore, as shown in Figure 8, the in vitro T_2-weighted images of the magnetic vesicles at various Fe concentrations

T_2-weighted MR image							
$C_{Fe,2}$(μM)	0	21	31	42	65	125	205

Figure 8. T_2-weighted MR images obtained from magnetic vesicles at different concentrations (the first imaging revealed in pure water).

were collected at a multiple spin−echo 2D imaging sequence. With the increase of the Fe concentrations, the luminance of the MR images presented darker and darker compared to the pure water (the first image) until it was completely unable to be distinguished ($C_{Fe} \geq 205$ μM), which further confirmed that this water-dispersible Fe_3O_4-decorated magnetic polymer vesicle can serve as an efficient T_2 contrast agent in MRI.

On the basis of the above results, in vivo MRI measurements of the Fe_3O_4-decorated magnetic vesicles were conducted. Figure 9a−h showed the time-dependent T_2-weighted MR images of the mice that were obtained preinjection and after intravenous injection of magnetic polymer vesicles. Compared with Figure 9a, which was acquired before the injection as a control, the muscle of neck and legs, liver, and spleen of the mice were observed quickly darkening after 4 min of the injection of the contrast agent, indicating that the magnetic vesicles were enriched among these organs and then took effect. After 13 min, the signal in spleen partially recovered to the initial state. At ca. 100 min, the mice were completely recovered, indicating the end of metabolism of the mice.

DOI: 10.1021/acsami.5b03222
ACS Appl. Mater. Interfaces 2015, 7, 14043−14052

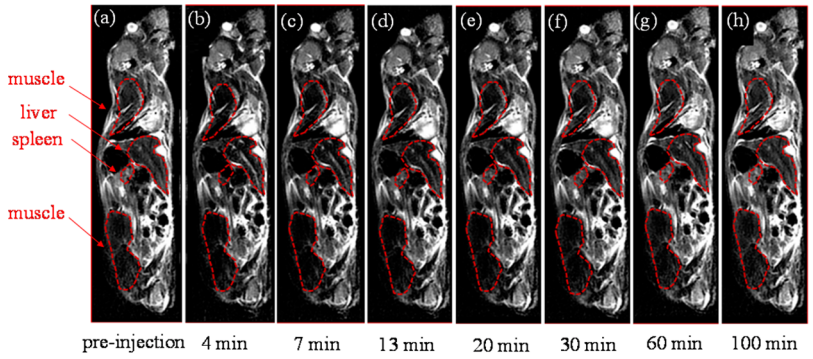

Figure 9. T_2-weighted MR images of the mice recorded (a) preinjection and (b–h) after injection of magnetic vesicles: (b) 4, (c) 7, (d) 13, (e) 20, (f) 30, (g) 60, and (h) 100 min.

3.7. Drug Loading and Release of Doxorubicin-Loaded Vesicles. To load the MRI contrast agent and the anticancer drug DOX·HCl into the same platform, we use two different ways to prepare DOX-loaded and Fe_3O_4-decorated magnetic vesicles.

One is mixing the anticancer drug (DOX·HCl) and the *preformed* Fe_3O_4-decorated vesicles (1.0 mg/mL) for 48 h. In this way, the DOX·HCl may penetrate through the vesicle membrane to reach the cavity of the vesicles or be adsorbed in the coronas of vesicles. The DLE is ca. 40.7%.

The other drug loading method is chemically precipitating the Fe_3O_4 nanoparticles in the DOX-loaded vesicles with a DLE of 20.5%, which is lower than that by the first method. The lower DLE is possibly because of the enhanced permeability of the PCL vesicle membrane at higher temperature, resulting in the loss of DOX·HCl during the Fe_3O_4 nanoparticles decoration at 60 °C.[51] On the other hand, drugs may be adsorbed in the vesicle coronas, rather than loaded in the cavity of vesicles by the first method. Also, the DOX-loaded vesicles without Fe_3O_4 nanoparticles with the highest DLE of 51.4% were prepared as a controlled group for comparison in the drug release experiments.

The experiments of DOX release were performed to evaluate the drug-delivery applications of the vesicles (without Fe_3O_4) and the magnetic vesicles (with Fe_3O_4) in 0.01 M tris buffer at pH 7.4 and 37 °C. As shown in Figure 10, curve (a) obtained from a control experiment of the free drug without vesicles or Fe_3O_4 exhibited rapid drug elution, as expected. Moreover, almost 80% of the DOX in the *preformed* magnetic vesicles was released in 4 h (curve (b)), indicating that the DOX may be mainly adsorbed in the vesicle coronas due to electrostatic interactions (rather than encapsulated in the cavity of vesicles). In contrast, the DOX-loaded vesicles with post Fe_3O_4 decoration (curve (c)) and DOX-loaded vesicles without Fe_3O_4 decoration (curve (d)) released only 50% and 30% of DOX within 4 h, respectively. Although the DOX-loaded magnetic vesicles with post Fe_3O_4 decoration shows lowest DLE, the slowest drug release rate at neutral pH indicates the best potential in drug-delivery applications because the toxic DOX are not prone to leakage in bloodstream, the release rate of DOX may be accelerated on demand such as in the presence of enzyme and acid conditions in tumor cells.

It is noteworthy that all curves do not reach the same maximum in Figure 10. In curve (b), the DOX·HCl may be mainly adsorbed in the coronas of vesicles due to electrostatic interactions between DOX and PAA coronas. In curve (c), this electrostatic interaction is weaker than that in curve (d) because

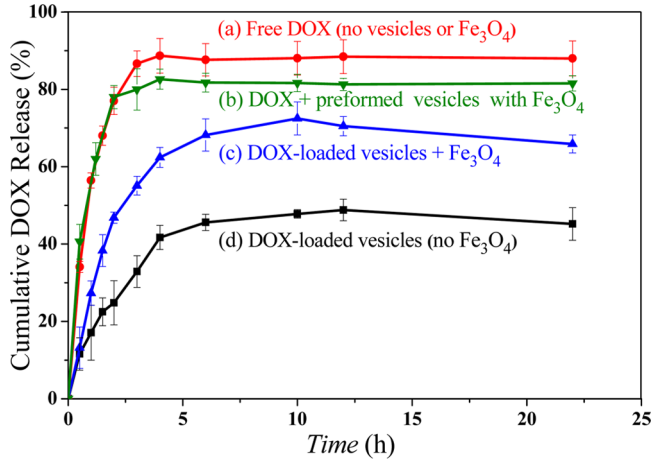

Figure 10. Cumulative release profile of (a) free DOX in the absence of vesicles or no Fe_3O_4 nanoparticles, (b) DOX-loaded magnetic vesicles by mixing DOX·HCl and the preformed magnetic vesicle, (c) DOX-loaded magnetic vesicles by loading DOX first then precipitating Fe_3O_4 nanoparticles; and (d) DOX-loaded vesicles (no Fe_3O_4) in 0.01 M tris buffer at pH 7.4 and 37 °C.

there are fewer carboxyl groups in the vesicles with Fe_3O_4 nanoparticles in curve (c). As a result, more DOX will be finally released from DOX-loaded vesicles in curve (c).

3.8. In Vitro Degradation. PCL is biodegradable with chain scission in the presence of *Pseudomonas* lipases, a kind of enzyme showing a high activity for ester chain scission.[52] The vesicles prepared from PEO_{43}-*b*-PCL_{98}-*b*-PAA_{25} triblock copolymer were subjected to enzymatic degradation of the central PCL block by *Pseudomonas* lipases. There are two basic steps in the enzymatic biodegradation: one is the adsorption of the lipase to the vesicles, and the other one is the interaction between the lipase and the PCL block.[53] Then, the vesicles are eventually degraded. Meanwhile, the Fe_3O_4 nanoparticles also can be degraded in the acid.[19]

The degradation of the same concentration of 100 and 50 μg/mL of pure vesicles and magnetic vesicles with 50 and 25 μg/mL lipase was monitored by the variation of the derived count rate by DLS (Figure 11). With the time going by, the derived count rate of the vesicle solution in the presence of lipase decreases gradually and finally reaches a plateau after 1 d. The polymer vesicles without Fe_3O_4 decoration were degraded by 93.3% (with 50 μg/mL of lipase) and 94.1% (with 25 μg/mL of lipase) after 25 h, while the degradation degree of Fe_3O_4-decorated vesicles was only 50.4% (with 50 μg/mL of lipase)

DOI: 10.1021/acsami.5b03222
ACS Appl. Mater. Interfaces 2015, 7, 14043–14052

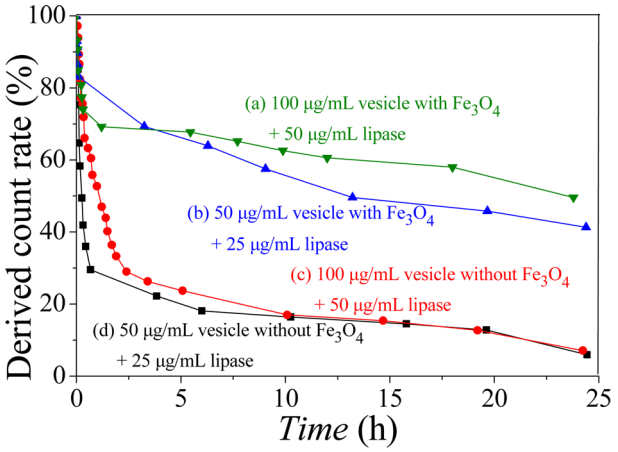

Figure 11. Derived count rate of vesicles with and without SPIONs with various copolymer concentrations as a function time in the presence of different enzyme concentraitons determined by DLS at 37 °C. (a) Vesicles with Fe_3O_4 nanoparticles (100 μg/mL) in the presence of lipase (50 μg/mL); (b) vesicles with Fe_3O_4 nanoparticles (50 μg/mL) in the presence of lipase (25 μg/mL); (c) vesicles without Fe_3O_4 nanoparticles (100 μg/mL) in the presence of lipase (50 μg/mL); (d) vesicles without Fe_3O_4 nanoparticles (50 μg/mL) in the presence of lipase (25 μg/mL).

and 48.7% (with 25 μg/mL of lipase), suggesting a slower degradation rate due to the influence of iron oxide.

Furthermore, we evaluated the degradation of Fe_3O_4 nanoparticles under acidic conditions. The concentration of free Fe ions outside the dialysis tube for vesicles was evaluated by ICP-MS, which was thus used to calculate the amount of intact Fe_3O_4 nanoparticles in the vesicles. As shown in Figure 12, the concentration of Fe in the vesicles (with ∼3.0 wt % SPIONs) gradually decreases with time in the tris buffer at pH 5.0 and 37 °C. After ∼52 h, 28.7% of the Fe_3O_4 was degraded, indicating that the Fe_3O_4 nanoparticles were transformed into iron ions.

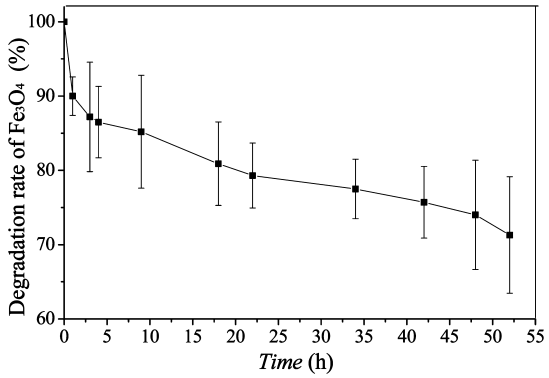

Figure 12. Time-dependent degradation of Fe_3O_4 nanoparticles decorated in the vesicles in tris buffer at pH 5.0 and 37 °C for 52 h.

4. CONCLUSIONS

In conclusion, we have successfully developed a new water-dispersible, biodegradable, biocompatible, and low cytotoxicity magnetic polymer vesicles for T_2-weighted MR imaging and anticancer drug delivery. The ultrafine SPIONs were grown among the vesicle coronas via in situ chemical precipitation. DLS, TEM, EDS, and VSM revealed the formation and morphology of the Fe_3O_4-decorated magnetic polymer vesicles. Furthermore, the CCK-8 assay revealed the low cytotoxicity against L02 cells. The in vitro and in vivo MR imaging experiments confirmed the T_2-weighted MR imaging function with an r_2 of 108.4 mM^{-1} s^{-1} and perfect metastasis in mice. Moreover, postprecipitation of Fe_3O_4 in the DOX-loaded vesicles leads to a slower release rate of DOX than the preformed Fe_3O_4-precipitated vesicles. In addition, both polymer vesicles and Fe_3O_4 nanoparticles showed degradability. Overall, our strategy by rationally growing ultrafine superparamagnetic Fe_3O_4 nanoparticles in the coronas of polymer vesicles provides a new insight for preparing promising biodegradable nanocarriers of theranostic agents for anticancer drug delivery and MR imaging.

■ ASSOCIATED CONTENT

Ⓢ Supporting Information

Calculation of Fe concentration in the degradation test. The Supporting Information is available free of charge on the ACS Publications website at DOI: 10.1021/acsami.5b03222.

■ AUTHOR INFORMATION

Corresponding Author

*E-mail: jzdu@tongji.edu.cn. Phone: +86-21-6958-0239. Fax: +86-21-6958-4723.

Notes

The authors declare no competing financial interest.

■ ACKNOWLEDGMENTS

J.D. is supported by National Natural Science Foundation of China (21174107 and 21374080), Eastern Scholar Professorship (P2009011), Shanghai 1000 Plan (SH01068), and the open fund of Beijing National Laboratory for Molecular Sciences (20140127).

■ REFERENCES

(1) Qiao, R. R.; Yang, C. H.; Gao, M. Y. Superparamagnetic Iron Oxide Nanoparticles: from Preparations to in Vivo MRI Applications. *J. Mater. Chem.* **2009**, *19*, 6274−6293.

(2) Jolesz, F. A. MRI-Guided Focused Ultrasound Surgery. *Annu. Rev. Med.* **2009**, *60*, 417−430.

(3) Na, H. B.; Song, I. C.; Hyeon, T. Inorganic Nanoparticles for MRI Contrast Agents. *Adv. Mater.* **2009**, *21*, 2133−2148.

(4) Bridot, J.-L.; Faure, A.-C.; Laurent, S.; Rivière, C.; Billotey, C.; Hiba, B.; Janier, M.; Josserand, V.; Coll, J.-L.; Vander Elst, L.; Muller, R.; Roux, S.; Perriat, P.; Tillement, O. Hybrid Gadolinium Oxide Nanoparticles: Multimodal Contrast Agents for in Vivo Imaging. *J. Am. Chem. Soc.* **2007**, *129*, 5076−5084.

(5) Carr, D. H.; Brown, J.; Bydder, G. M.; Weinmann, H. J.; Speck, U.; Thomas, D. J.; Young, I. R. Intravenous Chelated Gadolinium as A Contrast Agent in NMR Imaging of Cerebral Tumors. *Lancet* **1984**, *323*, 484−486.

(6) Laurent, S.; Forge, D.; Port, M.; Roch, A.; Robic, C.; Elst, L. V.; Muller, R. N. Magnetic Iron Oxide Nanoparticles: Synthesis, Stabilization, Vectorization, Physicochemical Characterizations, and Biological Applications. *Chem. Rev.* **2008**, *108*, 2064−2110.

(7) Szpak, A.; Fiejdasz, S.; Prendota, W.; Strączek, T.; Kapusta, C.; Szmyd, J.; Nowakowska, M.; Zapotoczny, S. T_1−T_2 Dual-Modal MRI Contrast Agents Based on Superparamagnetic Iron Oxide Nanoparticles with Surface Attached Gadolinium Complexes. *J. Nanopart. Res.* **2014**, *16*, 1−11.

(8) Do, M. A.; Yoon, G. J.; Yeum, J. H.; Han, M.; Chang, Y.; Choi, J. H. Polyethyleneimine-Mediated Synthesis of Superparamagnetic Iron Oxide Nanoparticles with Enhanced Sensitivity in T_2 Magnetic Resonance Imaging. *Colloids Surf., B* **2014**, *122*, 752−759.

DOI: 10.1021/acsami.5b03222
ACS Appl. Mater. Interfaces 2015, 7, 14043−14052

(9) Lu, Z.-R.; Wang, X.; Parker, D. L.; Goodrich, K. C.; Buswell, H. R. Poly(l-glutamic acid) Gd(III)-DOTA Conjugate with a Degradable Spacer for Magnetic Resonance Imaging. *Bioconjugate Chem.* **2003**, *14*, 715−719.
(10) Janib, S. M.; Moses, A. S.; MacKay, J. A. Imaging and Drug Delivery Using Theranostic Nanoparticles. *Adv. Drug Delivery Rev.* **2010**, *62*, 1052−1063.
(11) Bianchi, A.; Calabi, L.; Corana, F.; Fontana, S.; Losi, P.; Maiocchi, A.; Paleari, L.; Valtancoli, B. Thermodynamic and Structural Properties of Gd(III) Complexes with Polyamino-Polycarboxylic Ligands: Basic Compounds for the Development of MRI Contrast Agents. *Coordin. Chem. Rev.* **2000**, *204*, 309−393.
(12) Bernstein, E. J.; Schmidt-Lauber, C.; Kay, J. Nephrogenic Systemic Fibrosis: A Systemic Fibrosing Disease Resulting from Gadolinium Exposure. *Best Pract. Res., Clin. Rheumatol.* **2012**, *26*, 489−503.
(13) Sun, C.; Lee, J. S. H.; Zhang, M. Magnetic Nanoparticles in MR Imaging and Drug Delivery. *Adv. Drug Delivery Rev.* **2008**, *60*, 1252−1265.
(14) Lu, A. H.; Salabas, E. L.; Schuth, F. Magnetic Nanoparticles: Synthesis, Protection, Functionalization, and Application. *Angew. Chem., Int. Ed.* **2007**, *46*, 1222−1244.
(15) Neuberger, T.; Schöpf, B.; Hofmann, H.; Hofmann, M.; von Rechenberg, B. Superparamagnetic Nanoparticles for Biomedical Applications: Possibilities and Limitations of a New Drug Delivery System. *J. Magn. Magn. Mater.* **2005**, *293*, 483−496.
(16) Liu, Q. M.; Chen, S.; Chen, J.; Du, J. Z. An Asymmetrical Polymer Vesicle Strategy for Significantly Improving T_1 MRI Sensitivity and Cancer-Targeted Drug Delivery. *Macromolecules* **2015**, *48*, 739−749.
(17) Jain, T. K.; Richey, J.; Strand, M.; Leslie-Pelecky, D. L.; Flask, C. A.; Labhasetwar, V. Magnetic Nanoparticles with Dual Functional Properties: Drug Delivery and Magnetic Resonance Imaging. *Biomaterials* **2008**, *29*, 4012−4021.
(18) Chandra, V.; Park, J.; Chun, Y.; Lee, J. W.; Hwang, I. C.; Kim, K. S. Water-Dispersible Magnetite-Reduced Graphene Oxide Composites for Arsenic Removal. *ACS Nano* **2010**, *4*, 3979−3986.
(19) Li, D.; Zhang, Y.; Yu, M.; An, Q.; Guo, J.; Lu, J. Q.; Wang, C. A New Strategy for Synthesis of Porous Magnetic Supraparticles with Excellent Biodegradability. *Chem. Commun.* **2015**, *51*, 1908−1910.
(20) Sanson, C.; Diou, O.; Thevenot, J.; Ibarboure, E.; Soum, A.; Brulet, A.; Miraux, S.; Thiaudiere, E.; Tan, S.; Brisson, A.; Dupuis, V.; Sandre, O.; Lecommandoux, S. Doxorubicin Loaded Magnetic Polymersomes: Theranostic Nanocarriers for MR Imaging and Magneto-Chemotherapy. *ACS Nano* **2011**, *5*, 1122−1140.
(21) Brigger, I.; Dubernet, C.; Couvreur, P. Nanoparticles in Cancer Therapy and Diagnosis. *Adv. Drug Delivery Rev.* **2002**, *54*, 631−651.
(22) Maeda, H.; Wu, J.; Sawa, T.; Matsumura, Y.; Hori, K. Tumor Vascular Permeability and the EPR Effect in Macromolecular Therapeutics: a Review. *J. Controlled Release* **2000**, *65*, 271−284.
(23) Du, J. Z.; O'Reilly, R. K. Anisotropic Particles with Patchy, Multicompartment and Janus Architectures: Preparation and Application. *Chem. Soc. Rev.* **2011**, *40*, 2402−2416.
(24) Du, J. Z.; O'Reilly, R. K. Advances and Challenges in Smart and Functional Polymer Vesicles. *Soft Matter* **2009**, *5*, 3544−3561.
(25) Gao, Z.; Kennedy, A. M.; Christensen, D. A.; Rapoport, N. Y. Drug-Loaded Nano/Microbubbles for Combining Ultrasonography and Targeted Chemotherapy. *Ultrasonics* **2008**, *48*, 260−270.
(26) Chi, X. D.; Ji, X. F.; Xia, D. Y.; Huang, F. H. A Dual-Responsive Supra-Amphiphilic Polypseudorotaxane Constructed from a Water-Soluble Pillar[7]arene and an Azobenzene-Containing Random Copolymer. *J. Am. Chem. Soc.* **2015**, *137*, 1440−1443.
(27) Huang, P.; Wang, D. L.; Su, Y.; Huang, W.; Zhou, Y. F.; Cui, D. X.; Zhu, X. Y.; Yan, D. Y. Combination of Small Molecule Prodrug and Nanodrug Delivery: Amphiphilic Drug−Drug Conjugate for Cancer Therapy. *J. Am. Chem. Soc.* **2014**, *136*, 11748−11756.
(28) Hu, X. L.; Liu, G. H.; Li, Y.; Wang, X. R.; Liu, S. Y. Cell-Penetrating Hyperbranched Polyprodrug Amphiphiles for Synergistic Reductive Milieu-Triggered Drug Release and Enhanced Magnetic Resonance Signals. *J. Am. Chem. Soc.* **2014**, *137*, 362−368.
(29) Zhou, C. C.; Wang, M. Z.; Zou, K. D.; Chen, J.; Zhu, Y. Q.; Du, J. Z. Antibacterial Polypeptide-Grafted Chitosan-Based Nanocapsules As an "Armed" Carrier of Anticancer and Antiepileptic Drugs. *ACS Macro Lett.* **2013**, *2*, 1021−1025.
(30) Jones, C. H.; Chen, C.-K.; Jiang, M.; Fang, L.; Cheng, C.; Pfeifer, B. A. Synthesis of Cationic Polylactides with Tunable Charge Densities as Nanocarriers for Effective Gene Delivery. *Mol. Pharmaceutics* **2013**, *10*, 1138−1145.
(31) Ye, F.; Barrefelt, Å.; Asem, H.; Abedi-Valugerdi, M.; El-Serafi, I.; Saghafian, M.; Abu-Salah, K.; Alrokayan, S.; Muhammed, M.; Hassan, M. Biodegradable Polymeric Vesicles Containing Magnetic Nanoparticles, Quantum Dots and Anticancer Drugs for Drug Delivery and Imaging. *Biomaterials* **2014**, *35*, 3885−3894.
(32) Wang, H.; Wang, S.; Liao, Z.; Zhao, P.; Su, W.; Niu, R.; Chang, J. Folate-Targeting Magnetic Core−Shell Nanocarriers for Selective Drug Release and Imaging. *Int. J. Pharm.* **2012**, *430*, 342−349.
(33) Oh, J. K.; Park, J. M. Iron Oxide-Based Superparamagnetic Polymeric Nanomaterials: Design, Preparation, and Biomedical Application. *Prog. Polym. Sci.* **2011**, *36*, 168−189.
(34) Hong, R. Y.; Feng, B.; Chen, L. L.; Liu, G. H.; Li, H. Z.; Zheng, Y.; Wei, D. G. Synthesis, Characterization and MRI Application of Dextran-Coated Fe_3O_4 Magnetic Nanoparticles. *Biochem. Eng. J.* **2008**, *42*, 290−300.
(35) Rijcken, C. J. F.; Soga, O.; Hennink, W. E.; van Nostrum, C. F. Triggered Destabilisation of Polymeric Micelles and Vesicles by Changing Polymers Polarity: an Attractive Tool for Rrug Delivery. *J. Controlled Release* **2007**, *120*, 131−148.
(36) Ren, T. B.; Liu, Q. M.; Lu, H.; Liu, H. M.; Zhang, X.; Du, J. Z. Multifunctional Polymer Vesicles for Ultrasensitive Magnetic Resonance Imaging and Drug Delivery. *J. Mater. Chem.* **2012**, *22*, 12329−12338.
(37) Sanson, C.; Diou, O.; Thévenot, J.; Ibarboure, E.; Soum, A.; Brûlet, A.; Miraux, S.; Thiaudière, E.; Tan, S.; Brisson, A.; Dupuis, V.; Sandre, O.; Lecommandoux, S. Doxorubicin Loaded Magnetic Polymersomes: Theranostic Nanocarriers for MR Imaging and Magneto-Chemotherapy. *ACS Nano* **2011**, *5*, 1122−1140.
(38) Hickey, R. J.; Koski, J.; Meng, X.; Riggleman, R. A.; Zhang, P.; Park, S.-J. Size-Controlled Self-Assembly of Superparamagnetic Polymersomes. *ACS Nano* **2013**, *8*, 495−502.
(39) Liu, Q. M.; Chen, J.; Du, J. Z. Asymmetrical Polymer Vesicles with a "Stealthy" Outer Corona and an Endosomal-Escape-Accelerating Inner Corona for Efficient Intracellular Anticancer Drug Delivery. *Biomacromolecules* **2014**, *15*, 3072−3082.
(40) Yang, X. Q.; Grailer, J. J.; Rowland, I. J.; Javadi, A.; Hurley, S. A.; Steeber, D. A.; Gong, S. Q. Multifunctional SPIO/DOX-Loaded Wormlike Polymer Vesicles for Cancer Therapy and MR Imaging. *Biomaterials* **2010**, *31*, 9065−9073.
(41) Huang, J. S.; Wan, S. R.; Guo, M.; Yan, H. S. Preparation of Narrow or Mono-Disperse Crosslinked Poly((meth)acrylic acid)/Iron Oxide Magnetic Microspheres. *J. Mater. Chem.* **2006**, *16*, 4535−4541.
(42) Zhang, M.; Wang, B.; Zhang, Y.; B, H. Study on the Preparation of Magnetic Ction-Exchange Resins by Chemical Transformation. *Ion Exch. Adsorpt.* **1995**, *11*, 302−308.
(43) Gupta, A. K.; Gupta, M. Synthesis and Surface Engineering of Iron Oxide Nanoparticles for Biomedical Applications. *Biomaterials* **2005**, *26*, 3995−4021.
(44) Schutt, W.; Gruttner, C.; Hafeli, U.; Zborowski, M.; Teller, J.; Putzar, H.; Schumichen, C. Applications of Magnetic Targeting in Diagnosis and Therapy - Possibilities and Limitations: A Mini-Review. *Hybridoma* **1997**, *16*, 109−117.
(45) Mahmoudi, M.; Simchi, A.; Imani, M.; Milani, A. S.; Stroeve, P. Optimal Design and Characterization of Superparamagnetic Iron Oxide Nanoparticles Coated with Polyvinyl Alcohol for Targeted Delivery and Imaging. *J. Phys. Chem. B* **2008**, *112*, 14470−14481.
(46) Yang, X. Y.; Zhang, X. Y.; Ma, Y. F.; Huang, Y.; Wang, Y. S.; Chen, Y. S. Superparamagnetic Graphene Oxide-Fe(3)O(4) Nano-

DOI: 10.1021/acsami.5b03222
ACS Appl. Mater. Interfaces 2015, 7, 14043−14052

particles Hybrid for Controlled Targeted Drug Carriers. *J. Mater. Chem.* **2009**, *19*, 2710−2714.
(47) Yang, X. Q.; Grailer, J. J.; Rowland, I. J.; Javadi, A.; Hurley, S. A.; Matson, V. Z.; Steeber, D. A.; Gong, S. Q. Multifunctional Stable and pH-Responsive Polymer Vesicles Formed by Heterofunctional Triblock Copolymer for Targeted Anticancer Drug Delivery and Ultrasensitive MR Imaging. *ACS Nano* **2010**, *4*, 6805−6817.
(48) Lattuada, M.; Hatton, T. A. Preparation and Controlled Self-Assembly of Janus Magnetic Nanoparticles. *J. Am. Chem. Soc.* **2007**, *129*, 12878−12889.
(49) Berret, J. F.; Schonbeck, N.; Gazeau, F.; El Kharrat, D.; Sandre, O.; Vacher, A.; Airiau, M. Controlled Clustering of Superparamagnetic Nanoparticles Using Block Copolymers: Design of New Contrast Agents for Magnetic Resonance Imaging. *J. Am. Chem. Soc.* **2006**, *128*, 1755−1761.
(50) Rohrer, M.; Bauer, H.; Mintorovitch, J.; Requardt, M.; Weinmann, H. J. Comparison of Magnetic Properties of MRI Contrast Media Solutions at Different Magnetic Field Strengths. *Invest. Radiol.* **2005**, *40*, 715−724.
(51) Du, J. Z.; Tang, Y. Q.; Lewis, A. L.; Armes, S. P. pH-Sensitive Vesicles Based on a Biocompatible Zwitterionic Diblock Copolymer. *J. Am. Chem. Soc.* **2005**, *127*, 17982−17983.
(52) Żenkiewicz, M.; Richert, A.; Malinowski, R.; Moraczewski, K. A Comparative Analysis of Mass Losses of Some Aliphatic Polyesters upon Enzymatic Degradation. *Polym. Test.* **2013**, *32*, 209−214.
(53) Zou, K. D.; Liu, Q. M.; Chen, J.; Du, J. Z. Silver-Decorated Biodegradable Polymer Vesicles with Excellent Antibacterial Efficacy. *Polym. Chem.* **2014**, *5*, 405−411.

DOI: 10.1021/acsami.5b03222
ACS Appl. Mater. Interfaces 2015, 7, 14043−14052